Single-well imaging using the full waveform of an acoustic sonic

Louis Chabot, David C. Henley, and R. James Brown

ABSTRACT

This work looks at single-well imaging using the full waveform as acquired by an acoustic well-logging tool. This work begins by presenting the known theory of the propagation of acoustic waves in a fluid-filled borehole. Next, with the help of 2-D numerical finite-difference modelling, an insight into the theory is developed. Once this step is completed, a scaled physical model of a borehole is to be built, in which full waveform surveys will be conducted to understand the 3-D nature of the problem. After those numerical and physical studies are completed, techniques will be developed for the processing of the full waveforms into "images". Those methods will be calibrated and tested not only on simulated data sets but also on real field data sets. The ultimate goal of this work is to image acoustic-impedance anomalies beyond the borehole wall and thus gain a better picture of the reservoir characteristics around the borehole.

INTRODUCTION TO ACOUSTIC BOREHOLE IMAGING

Today, borehole seismology comes in different forms: tomography or cross-well imaging (transmitter in one borehole and receiver in another), vertical seismic profiling (transmitter on the surface and receiver in a borehole), and single-well imaging (transmitter and receiver in the same borehole). Single-well imaging is practised in different ways. There is single-well imaging using a borehole seismic source with clamped receivers in the same borehole, for example, to image the flank of a salt dome and there is single-well imaging using a well-logging tool, for example, to characterize the elastic properties of a geologic formation. The focus of this work is on the latter. Borehole imaging devices can provide valuable information to aid in reservoir description. Applications include fracture identification, stratigraphic interpretation, imaging nearby sand channels and delineating steam-flood fronts.

An active example of single-well imaging is the acoustic imaging of borehole walls. The Baker Hughes Circumferential Borehole Imaging Log or CBIL™ is produced using a circumferential borehole imaging device that utilizes a rotating transducer operating in a pulse-echo mode (ultrasonic 250 kHz) to scan the entire circumference of the borehole wall. An independent sensor section measures mud traveltime so that travel length can be calculated. Travel lengths calculated at each cardinal compass point (N, S, E and W) provide a 4-arm caliper record of the borehole. Variations in lithology, physical rock features (fractures, vugs) and borehole geometry cause changes in the measured amplitudes and traveltimes, collectively providing a map or image of the borehole wall (Faraguna et al., 1989).

Can we look deeper and beyond the borehole walls with single-well imaging?

As an example of work done to date, Hornby (1989) used an acoustic well-logging tool equipped with one monopole source and 12 receivers, each recording 20 ms of full waveform data, to compute an image of structural changes beyond the borehole wall. With the source and receiver array both passing through the structures that cross the borehole, downdip and updip structures could be imaged separately.

Since the work done by Hornby in 1989, acoustic well-logging technologies have much evolved. Now well-logging tools are not only built with a longer spacing, enabling them to look deeper into the formation, but also are equipped with electronics that provide them with the ability to better record the full waveform. Also, better processing technologies enable the successful identification of not only compressional, but also shear and Stoneley arrivals.

The objective of this project is to further explore the use of the full sonic wavetrain in detecting and imaging scattered energy beyond the borehole wall.

THEORY

The theory of acoustic-wave propagation in a fluid-filled borehole has been covered in some textbooks (e.g. Bourbie et al., 1987). "An omnidirectional pressure source creates a compressional wave pulse in the borehole fluid, which propagates out into the formation. As this pulse enters the formation, it creates a slight uniform bulge around the borehole wall. This in turn excites both compressional and shear waves in the formation" (Schlumberger, 1997). As the compressional and shear waves propagate in the formation, they generate head waves in the borehole fluid (at critical incidence) and thus refracted arrivals. "Trailing the head waves are the more complicated guided borehole waves and the Stoneley wave. The guided borehole waves come from reflections of source waves reverberating in the borehole" (Schlumberger, 1997). The Stoneley wave, an interface wave guided by the borehole that decays from both sides of the fluid/solid interface, travels more slowly than the fluid waves. Far-field velocities are associated with geophysical measurements (surface seismic ties) while near-field velocities are associated with geomechanical properties (borehole annulus).

NUMERICAL MODELLING

To verify the theory and yield insight into the propagation of waves from a monopole source in a fluid-filled borehole, the first step in this project was to conduct numerical modelling of acoustic-wave propagation in a fluid-filled borehole. There are several finite-difference algorithms available. For this particular application, a finite-difference modelling code was selected where the formulation is 4th order in space and 2nd order in time. The finite-difference code was provided to us by G.T. Schuster, J. Xu and Y. Luo (University of Utah) and is based on an algorithm described by Levander (1988). Additional modifications to the code have been made by S. Guevara (CREWES). The advantages of the staggered-grid scheme of this algorithm lie in its stability and accuracy for modelling materials with large Poisson's ratio and mixed acoustic-elastic media (Levander, 1988).

The numerical model attempts to replicate the borehole environment. The model presented here is a two-dimensional one, characterized by a horizontal fluid layer confined both above and below by two identical elastic layers. This horizontal fluid layer simulates the borehole. The model is scaled to emulate the geometric relationships in a borehole. The source emitted is defined as a line source (geometrical characteristics) with a 30-Hz Ricker wavelet with duration of 130 ms (time signal). The source is located at the left end of the borehole axis. "Geophones" are placed on the borehole axis to record the particle velocity. The results of the finite-difference modelling are presented with Matlab™.

Assuming cylindrical geometry and an idealized borehole, a series of snapshots of the wavefield generated by the finite-difference calculation are presented in Figure 1.

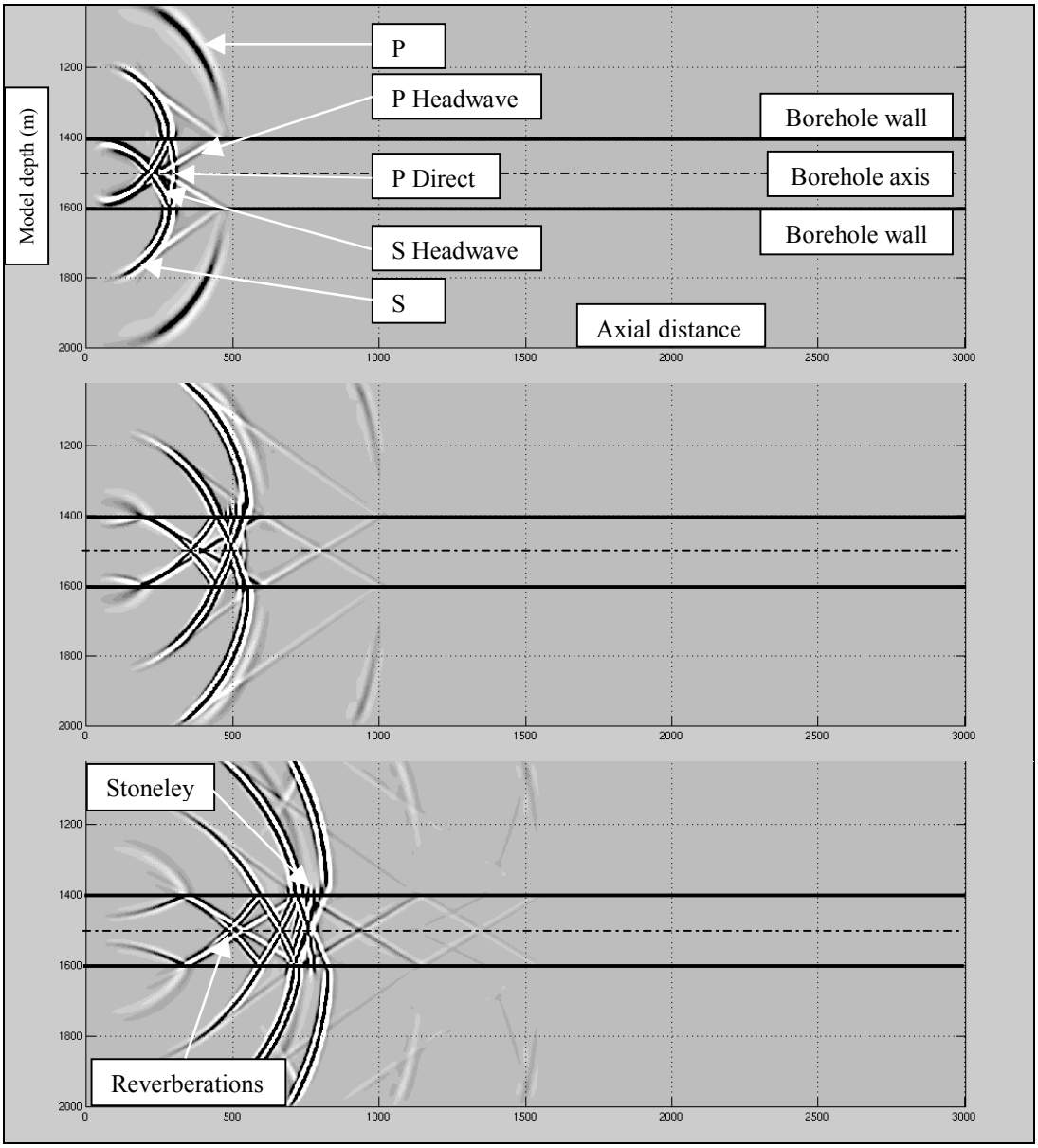

Figure 1. Snapshots of the particle velocity wavefield (vertical component) at 400 ms (top), 700 ms (middle) and 1000 ms (bottom).

These snapshots display the acoustic field in the borehole and the elastic field in the surrounding formation. The left and bottom scales are model depth and axial distance in metres. Undisturbed borehole fluid and formation are uniform grey. Acoustic and elastic vertical components of particle velocity in the borehole fluid and formation are represented on a grey scale from white (negative) to black (positive). The effect of the well-logging tool is not accounted for in this numerical model. Details of the model are presented in Appendix A.

When looking at the series of snapshots, the generation of the direct P and the P and S headwaves in the fluid can be observed. Behind the headwaves in the borehole are the guided borehole waves and the Stoneley wave. The guided borehole waves are generated from the source pulse in the borehole fluid which is reflected from the formation many times. With each reflection, compressional and shear waves are excited in the formation. Also, one can observe the evanescent nature of the Stoneley wave, which travels along the borehole wall more slowly than the fluid wave.

Figure 2 illustrates a shot record of the vertical component of particle velocity at the "geophones" along the borehole axis of the direct P wave, P reflection, P and S headwaves, Stoneley and normal-mode arrivals.

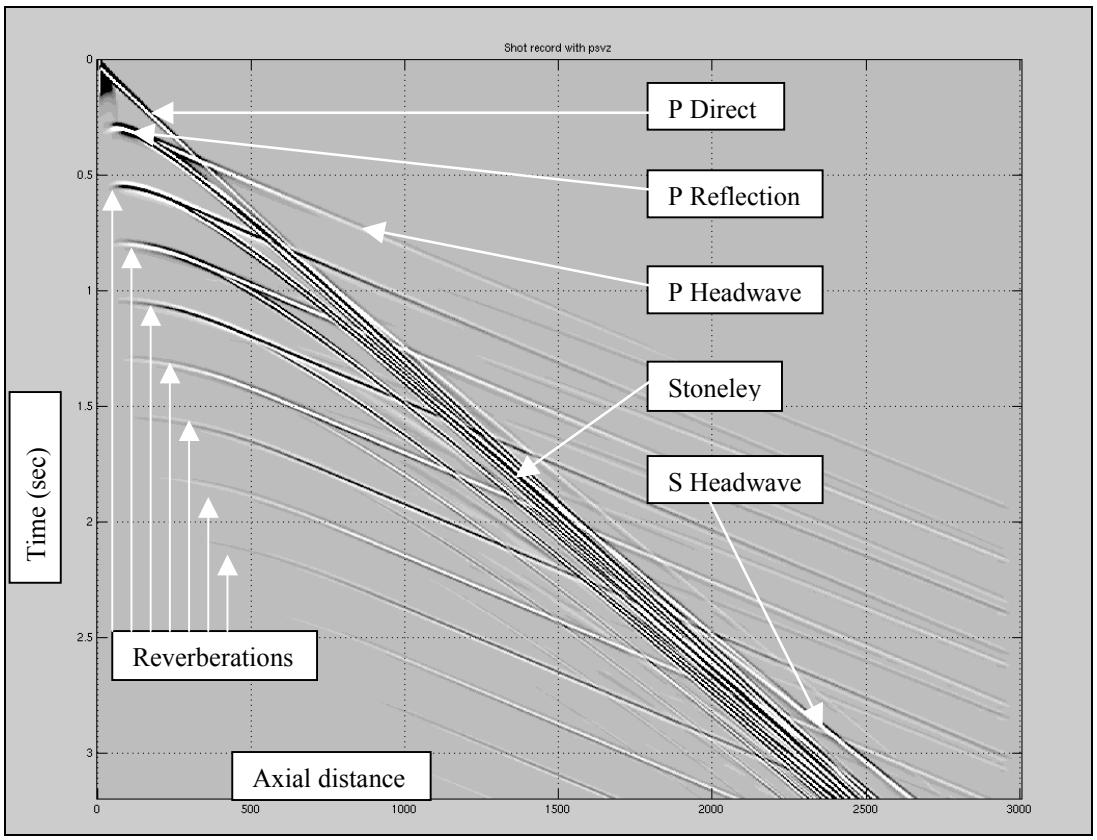

Figure 2. Shot record recorded along the borehole axis.

Further modifications to this finite-difference modelling code will be necessary in order to obtain the pressure response at the hydrophones instead of the particle velocity at the "geophones" of the well-logging tool.

PHYSICAL MODELLING

Following the 2-D numerical modelling, physical modelling will be conducted in order to fill the gap between the theory and the field environment. Physical modelling in the laboratory is conducted to check the predictions of the mathematician and to act as a direct aid in the interpretation of actual field records (Ebrom, 1994). Also the problem investigated is 3-D in nature and would naturally benefit from 3-D modelling.

In building a physical model we need to select the proper building material. In the selection of the building material, it will be important to select one whose shear-wave velocity is faster than the compressional-wave velocity in the fluid. This is critically important in order to observe shear waves in the wavetrain. To date we have tested 15 different wood materials. Because of the anisotropic nature of the wood tested, that material will not be retained at this point. Instead, a scaled model built of concrete is proposed with a scaling factor of 1:30 in dimensions of length (Chen, 1982). The model will be large enough to avoid boundary effects. This first scaled model will be homogeneous and isotropic to test the experimental set-up. Spherical transducers will be used as acoustic sources and receivers; both suspended in the fluid-filled borehole. If tests are successful, other physical models will follow, having specific geologic anomalies. The ratio of lengths of geological features to wavelength will be the same both in the field and in the model. The physical testing will be conducted at the CREWES physical modelling laboratory at the University of Calgary.

WAVEFORM PROCESSING - IMAGING

To date, no new algorithms have been proposed to process sonic waveforms. This step will be complete only when both the numerical and the theoretical modelling are successfully completed. In his imaging efforts, Hornby (1989) proposed the removal of direct P waves, P and S headwaves as well as the Stoneley arrivals with the use of an *f-k* filter. He then applied an acoustic back-projection operator to the prestack sonic velocity filtered data, followed by a 6-fold CMP stack. Finally, he migrated the data with a generalized Radon transform. Our efforts will initially follow a similar approach. In the meantime, an experiment in waveform processing using field data is presented in the next section.

FIELD DATA ANALYSIS

Any processing methods and algorithms developed in the previous section will be calibrated and tested not only on simulated and modelled data sets but also on real field data sets.

To date we have secured several full waveform data sets from the field for calibrating and testing processing techniques. Those full waveform data sets have been acquired at PanCanadian Blackfoot 8-8-23-23W4 and Garrington 11-3-37-5W5 wells and at Husky Pike's Peak 20868 and 25152 wells.

The full-waveform data sets at the PanCanadian wells were acquired with the Schlumberger Dipole Shear Sonic Imager or DSI™ well-logging tool (Figure 3). The two data sets, one for each well, were acquired in a monopole configuration. The monopole transmitter was operated at a centre frequency of 12 kHz. Receivers are located 15 cm apart on the tool with a near offset distance to the source of 2.74 metres. Eight full waveforms were recorded simultaneously at the firing of the monopole source. Each waveform was recorded with a sample interval of 10 μs for a total of 512 samples/waveform (Harrison et al., 1990).

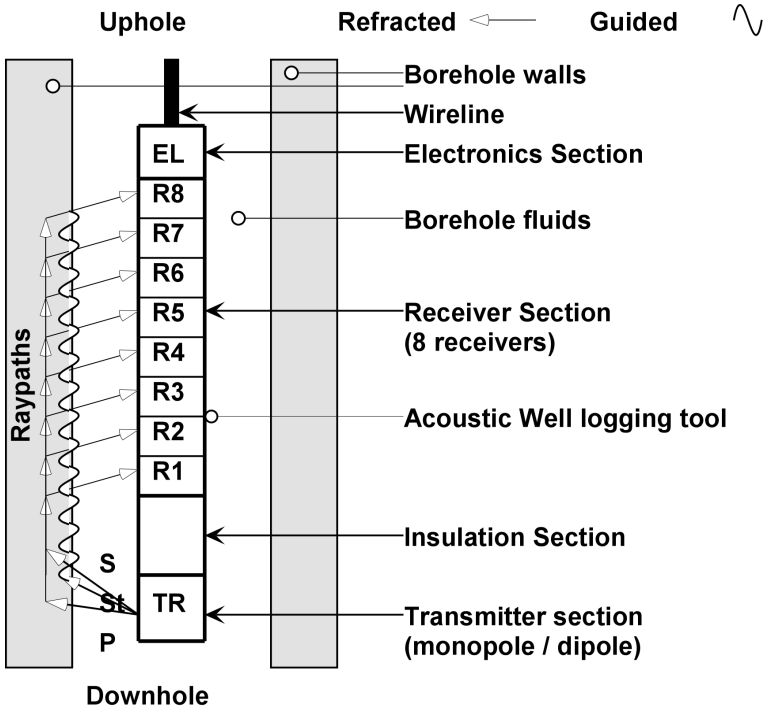

Figure 3. Diagram representing the acoustic well-logging tool DSI™, which was used to acquire the PanCanadian full-waveform data sets (modified after Schlumberger, 1997).

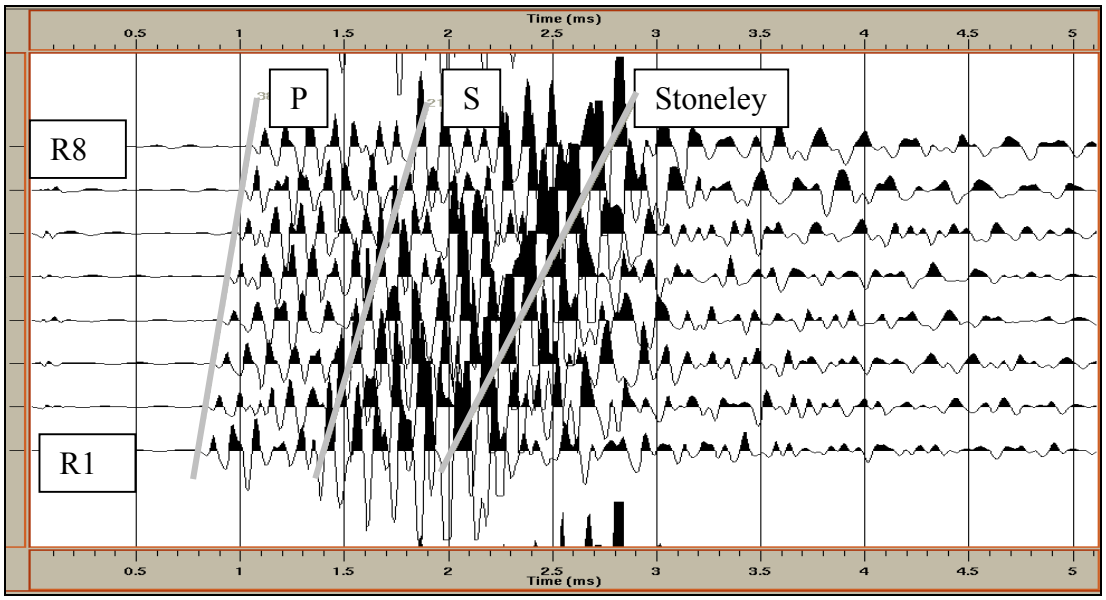

Figure 4. Identification of P, S and Stoneley arrivals in the acquired full waveform.

Figure 4 illustrates eight full waveforms simultaneously recorded in a single firing of the monopole source of the DSI™ well-logging tool. This sample of eight full waveforms was taken with a source depth of 1422.73 m from the PanCanadian Blackfoot 8-8-23-23W4 well. An initial look at this sample reveals the presence in the full waveform of the predicted compressional (at 3810 m/s), shear (at 2177 m/s) and Stoneley (at 1226 m/s) arrivals.

The full-waveform data sets at the Husky wells were acquired with the Computalog Monopole Dipole Array or MDA™ well-logging tool. The four data sets, two for each well, were acquired either in a monopole or in a dipole configuration. The monopole transmitter was operated at a centre frequency of 8 kHz. Four full waveforms were recorded simultaneously at the firing of the monopole source. Each waveform was recorded with a sample interval of 20 μs. The dipole transmitter was operated at a centre frequency of 2 kHz. Four full waveforms were recorded simultaneously at the firing of the dipole source. Each waveform was recorded with a sample interval of 40 μs.

In order to experiment with seismic processing, a full-waveform trace set was selected from the Husky data sets. The processing flow, as described in Figure 5, was applied to this trace set in order to attempt to resolve scattered energy recorded in the full waveform coming from beyond the borehole wall.

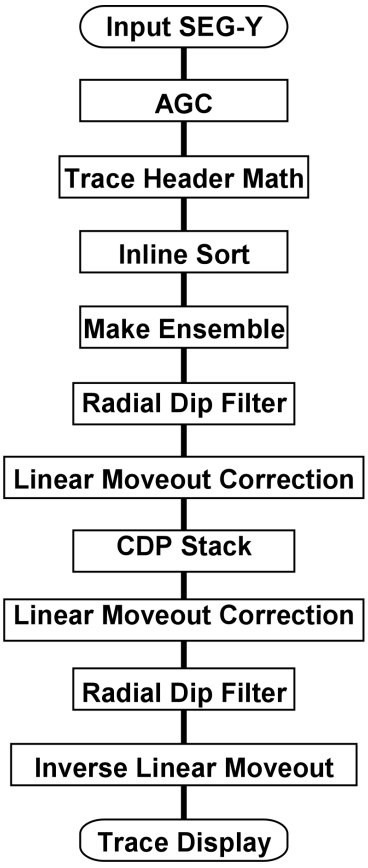

Figure 5. Processing flow applied to the Husky well full waveform trace set.

In detail, this processing flow consisted in the following steps. After data input and AGC, the trace header math helped to create the proper trace headers with geometry, CDP bins, offsets, etc. The inline sort gathered data into CDP gathers. In this test, the entire data set was made into one ensemble for linear event filtering. The radial dip filter was applied to filter out energy with the velocities of direct P, direct S, or tube wave (Henley, 1999a). The linear moveout correction was applied to correct the data for reflection/diffraction moveout, which is linear for this small range of offsets. After the CDP stack, another linear moveout correction was applied to give events parallel to the borehole a finite velocity. Again a radial dip filter was applied to filter out energy parallel to the borehole (Henley, 1999b). Inverse linear moveout, which undoes the previous linear moveout, was then applied. The energy left in the display should be mostly diffraction and reflections from any interfaces not parallel to the borehole.

Figure 6 shows the result of this processing flow. It can be observed that the residual energy is primarily reflected energy from irregularities in the borehole wall (near 4 ms) and scatterers farther away from the borehole wall (greater than 4 ms). The processing of the trace set provides an unmigrated first image.

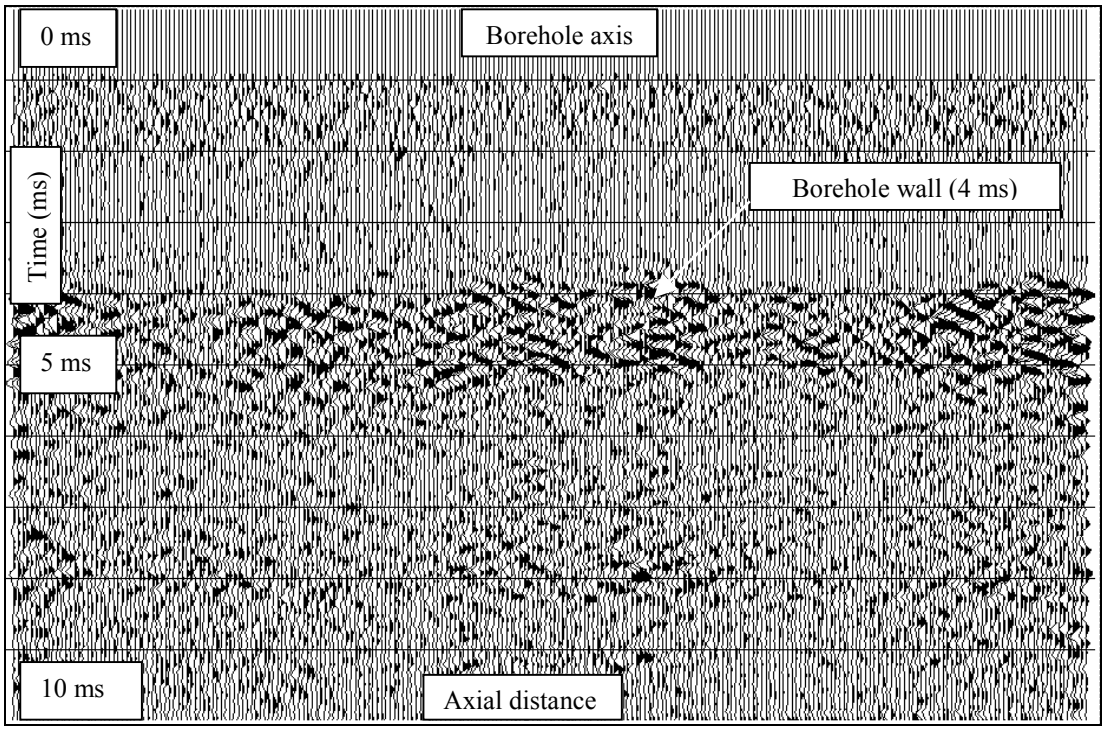

Figure 6. Diffractions and reflections (unmigrated) (data courtesy of Husky Energy Inc.).

The results from this processing experiment have yet to be compared with either the geology as interpreted in the well bore or from a geologic cross-section.

ACKNOWLEDGEMENTS

We would like to thank the CREWES sponsors for their financial assistance in this work. We would like also to thank PanCanadian Petroleum Ltd., Husky Energy Inc., Schlumberger Ltd. and Computalog Ltd. for providing us with the field data sets.

REFERENCES

Bourbie, T., Coussy, O., and Zinszner, B., 1987, Acoustics of porous media: Gulf Publishing, Houston, 334.

Chen, S.T., 1982, The full acoustic wave train in a laboratory model of a borehole: Geophysics, **47**, 1512 - 1520.

Ebrom, D.A., and McDonald, J.A., 1994, Seismic physical modelling: Geophysics reprint series No. 15.

Faraguna, J.F., Chace, D.M., and Schmidt, M.G., 1989, An improved borehole televiewer system – image acquisition, analysis and integration: Society of Professional Well Log Analysts Annual Logging Symposium, Denver, Colorado, Transactions.

Harrison, A.R., Randall, C.J., Aron, J.B., Morris, C.F., Wignall, A.H., Dworak, R.A., Rutledge, L.L., and Perkins, J.L., 1990, Acquisition and analysis of sonic waveforms from a borehole monopole and dipole source for the determination of compressional and shear speeds and their relation to rock mechanical properties and surface seismic data: SPE 20557.

Henley, D.C., 1999a, Coherent noise attenuation in the radial trace domain: Introduction and demonstration: CREWES Research Report, **11**, 455-491.

Henley, D.C., 1999b, Demonstration of radial trace domain filtering on the Shaganappi 1998 2-D geotechnical survey: CREWES Research Report, **11**, 787-803.

Hornby, B.E., 1989, Imaging of near-borehole structure using full-waveform sonic data: Geophysics, **54**, 747-757.

Levander, A.R., 1988, Fourth-order finite-difference P-SV seismograms: Geophysics, **53**, 1425-1436.

Schlumberger, 1997, DSI™ – Dipole Shear Sonic Imager: Corporate brochure SMP-9200, 36 pages.

APPENDIX A

Finite-Difference Parameters used for the model

Number of grid points in horizontal direction	2400	
Number of grid points in vertical direction	801	
Time step , space step (horizontal,vertical)	0.0004 s, 1.25 m	
Number of time steps	8000	
Peak frequency of Ricker wavelet	30.00 Hz	
Time step skipped , trace skipped	5 , 4	
Source/Receiver Parameters		
Source Coordinates (nxs,nzs)	5 , 400	
Geophone Depth	400	
Z-component source particle velocity		
Line Source		
No Free Surface		
Layer Parameters		
Parameters for Layer1		
Model compressional velocity	1800.00 m/s	
Model shear velocity	900.00 m/s	
Model density	2000.00 kg/m^3	
Parameters for Layer 2		
Model compressional velocity	800.00 m/s	
Model shear velocity	0.0 m/s	
Model density	1000.00 kg/m^3	
Parameters for Layer 3		
Model compressional velocity	1800.00 m/s	
Model shear velocity	900.00 m/s	
Model density	2000.00 kg/m^3	
Stability and Dispersion Information		
Maximum, Minimum velocity	1800.00 , 800.00	
Minimum Wavelength Criterion > 5*dx:	10.6667 > 6.25000	
Stability Criterion: .606 > cmax*dt/dx	0.576000	
Interface Node Information		
(x, z) =	(0.0,0.0)	layer = 1
(nx,nz) =	(1.00,1.00)	
(x, z) =	(3000.00,0.0)	layer = 1
(nx,nz) =	(2401.00,1.00)	
(x, z) =	(0.0,400.00)	layer = 2
(nx,nz) =	(1.00,321.00)	
(x, z) =	(3000.00,400.00)	layer = 2
(nx,nz) =	(2401.00,321.00)	
(x, z) =	(0.0,600.00)	layer = 3
(nx,nz) =	(1.00,481.00)	
(x, z) =	(3000.00,600.00)	layer = 3
(nx,nz) =	(2401.00,481.00)	